True-amplitude Kirchhoff migration, topography, and irregular acquisition geometry

C. Jäger, T. Hertweck, and M. Spinner

email: *Christoph.Jaeger@gpi.uka.de*

keywords: *migration, true amplitudes, irregular acquisition geometry, acquisition footprint, topography*

ABSTRACT

In areas with topographic variations, acquisition and processing of seismic data is a challenging task for exploration geophysicists. Although there exist methods to adjust the measured data to a flat datum, it is sometimes advantageous or even mandatory to migrate the data directly from topography in order to get high-quality migrated images. Apart from the direct effects of a non-flat measurement surface, the data processing is often further complicated due to an irregular measurement geometry. Kirchhoff migration is a suitable tool to handle such data in an efficient and amplitude-preserving way. However, several important aspects must be considered: migration weights must refer to the actual topographic measurement surface and its local dip and need to honor the local acquisition geometry. In addition, a careful estimation of the velocity model and the traveltime tables is necessary. Then, Kirchhoff true-amplitude prestack migration does not only produce kinematically correct images but also enables further studies that rely on the dynamic information of the migration output. A prominent example for such investigations is the analysis of amplitude variation with offset or angle in the prestack migrated images.

INTRODUCTION

Migration is an important step in the processing of seismic reflection data. In the course of the years, migration algorithms have much improved and prestack migrated data serve nowadays, in addition to providing a structural image, also as input for further analyses, e. g., amplitude versus offset (AVO) or amplitude versus angle (AVA) studies.

One of the oldest but also one of the most frequently used migration methods is Kirchhoff migration. Its algorithmic framework has been laid by Hagedoorn (1954) who presented a graphical migration scheme based on surfaces of maximum convexity. His work was later related to the wave equation and became familiar as Kirchhoff migration (Schneider, 1978). Kirchhoff depth migration treats each point M in the subsurface on a sufficiently dense grid like a diffraction point. In an a-priori given macrovelocity model, the relevant part of the Green's function of a point source at any single diffraction point M in the depth domain is calculated. The kinematic part of this Green's function is the configuration-specific diffraction traveltime surface. The migration output that is assigned to a depth point M is obtained by stacking the amplitudes of the filtered input seismogram along this surface. This explains why the Kirchhoff migration scheme is also called diffraction-stack migration. If desired, the effect of geometrical spreading can be removed from the output amplitudes by multiplying the data during the stack with a true-amplitude weight factor that can be calculated from the dynamic part of the Green's function. Then, the amplitudes in the obtained so-called true-amplitude migration result can serve as a measure for the angle-dependent reflection coefficient provided that other influences on the amplitude such as, e. g., transmission loss or source/receiver coupling effects are modest or can be corrected for.

In the last decades, many different migration algorithms have been developed; a rather complete discussion of the advantages and disadvantages of established methods can be found in Gray et al. (2001).

Although it has turned out that some of these methods can, at least in some scenarios, produces better images, the Kirchhoff method is still a competitive and widely investigated tool. The question is why? To answer this question, let us briefly summarize some properties of Kirchhoff migration: (1) The kinematic, i. e., traveltime-related, aspects of the method are easy to understand and to describe by means of Hagedoorn's shoestring migration approach (Bleistein, 1999). This allows, e. g., to explain artifacts that can arise in the context of limited-aperture Kirchhoff migration in a geometrical way (Hertweck et al., 2003). (2) Kirchhoff migration is able to handle vertically and laterally inhomogeneous media and provides in most cases reliable and accurate results while being efficient at the same time. (3) The method allows to image dips in the subsurface that are larger than 90 degrees. This handling of turning rays depends, however, on the method used to calculate the relevant Green's functions. (4) The migration technique is very flexible and allows the target-oriented processing of seismic data. (5) Kirchhoff migration can readily handle measurement surfaces with topographic variations and, closely related, irregular acquisition geometries without the need of redatuming or data regularization. This can be advantageous as was pointed out by Gray and Marfurt (1995). In the following sections, we will show that migration of such irregular data does not only yield a kinematically correct image of the subsurface, but can be applied in the above described true-amplitude sense, thus providing an output suitable for AVO/AVA analyses.

Mathematically, the Kirchhoff migration process is expressed as an integration over the recorded wavefield and reads in the 3D case (Schleicher et al., 1993)

$$V(M) = \frac{-1}{2\pi} \iint\limits_{A} d\xi_1 d\xi_2 \; W_{3D}(\xi_1, \xi_2, M) \frac{\partial U(\xi_1, \xi_2, t)}{\partial t}\bigg|_{t=\tau_D(\xi_1, \xi_2, M)} , \tag{1}$$

where $V(M)$ is the value assigned to one diffraction point M in the depth domain after migration and $U(\xi_1, \xi_2, t)$ denotes the principal component of the data in the time domain (seismogram). These data are assumed to consist of analytic (complex) traces which are formed by the actual traces recorded in the field as the real parts and their Hilbert transforms as the imaginary parts. In this way, migration by equation (1) correctly treats the phase shifts due to complex reflection coefficients (supercritical reflections) and possible caustics along the ray paths. The vector $\vec{\xi} = (\xi_1, \xi_2)$ is the so-called configuration parameter and represents the trace position. Sources and receivers are grouped into pairs, whose locations are described as a function of $\vec{\xi}$. The actual form of this function depends on the measurement configuration. The migration aperture A is the region over which $\vec{\xi}$ varies to cover all source-receiver pairs used in the stack. The factor $W_{3D}(\xi_1, \xi_2, M)$ is the true-amplitude weight function needed for the compensation of the geometrical spreading effect. This weight may (true-amplitude migration) or may not (purely kinematic migration) be included in the migration scheme. The stacking surface $t = \tau_D(\xi_1, \xi_2, M)$ is the diffraction traveltime surface for the depth point M. The time derivative $\partial U/\partial t$ is needed in order to correctly recover the source pulse (Newman, 1975).

In the 2.5D case where the model parameters are assumed to vary only with respect to the direction parallel to the seismic acquisition line (inline direction), the integral in the perpendicular direction (crossline direction) can be solved by the method of stationary phase. Thus, the stacking surfaces shrink to lines and the resulting formula for 2.5D Kirchhoff migration reads (Martins et al., 1997)

$$V(M) = \frac{1}{\sqrt{2\pi}} \int\limits_{A} d\xi \; W_{2.5D}(\xi, M) \; \partial t^{1/2} U(\xi, t)\big|_{t=\tau_D(\xi, M)} , \tag{2}$$

where $\partial t^{1/2}$ denotes the Hilbert transform of the time half-derivative. This is the 2.5D filter operation corresponding to the time derivative applied in the 3D case.

In all practical implementations of Kirchhoff migration, the integrals in equations (1) and (2) are realized by a summation process, the variables of integration $d\xi_1 d\xi_2$ and $d\xi$ are replaced by the discrete quantities $\Delta\xi_1 \Delta\xi_2$ and $\Delta\xi$, respectively. The resulting equation for 3D is

$$V(M) = \frac{-1}{2\pi} \sum\sum \Delta\xi_1 \Delta\xi_2 \; W_{3D}(\xi_1, \xi_2, M) \; \frac{\partial U(\xi_1, \xi_2, t)}{\partial t}\bigg|_{t=\tau_D(\xi_1, \xi_2, M)} , \tag{3}$$

and the corresponding expression for 2.5D reads

$$V(M) = \frac{1}{\sqrt{2\pi}} \sum \Delta\xi \; W_{2.5D}(\xi, M) \; \partial t^{1/2} U(\xi, t)\big|_{t=\tau_D(\xi, M)} . \tag{4}$$
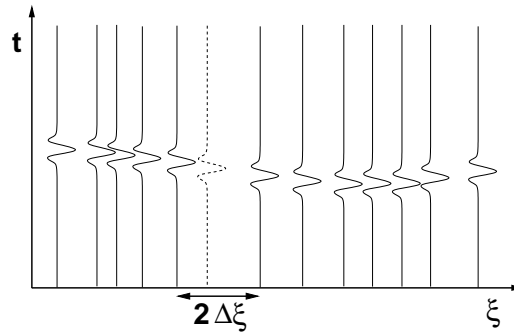
Figure 1: Determination of the local trace weighting factor $\Delta\xi$ in 2.5D poststack migration. The dashed trace is weighted by half the midpoint distance between its neighboring traces.

TOPOGRAPHY AND IRREGULAR ACQUISITION GEOMETRY

For migration of data recorded with an irregular measurement geometry and/or on a non-flat measurement surface, several aspects have to be considered:

- For the computation of the traveltimes (necessary for the construction of the stacking operator τ_D) the actual topographic measurement surface must be taken into account. This is fundamental, no matter if one is interested in "true" amplitudes or if a purely kinematic migration is to be performed.

- The true-amplitude weight function must refer to the actual measurement surface. A detailed derivation of a true-amplitude weight that is valid for migration from topography was carried out by Spinner (2003), see also Jäger et al. (2003).

- Irregular acquisition geometries result in non-constant factors $\Delta\xi_1\Delta\xi_2$ or $\Delta\xi$, respectively. If we look at equations (3) and (4), it is obvious that these quantities affect the amplitudes of the migration result. Therefore, each input trace has to be weighted, in addition to the true-amplitude weight function, by a local estimate of $\Delta\xi_1\Delta\xi_2$ or $\Delta\xi$, respectively, in order to yield output amplitudes that are not falsified by the irregular geometry. Furthermore, ignoring an irregular acquisition geometry leads to artifacts known as acquisition footprint.

Determination of the trace spacing $\Delta\xi_1\Delta\xi_2$ and $\Delta\xi$

Weighting the input traces by a quantity that accounts for an irregular acquisition geometry is known as acquisition footprint removal in the literature (Canning and Gardner, 1998; Jousset et al., 1999, 2000). For 2.5D poststack migration, the determination of a local $\Delta\xi$ is quite simple (Figure 1). Assuming that all traces in the poststack dataset are sorted with respect to ξ which could be, e. g., the midpoint coordinate, each trace is weighted by half the distance between the two neighboring traces, i. e., with

$$\Delta\xi_i = \frac{\xi_{i+1} - \xi_{i-1}}{2}, \quad i = \text{trace number} . \tag{5}$$

For 2.5D prestack migration, $\Delta\xi$ can be determined in a similar way. For a prestack or common-offset (CO) migration, the input is divided into offset bins; all traces inside such a bin are then migrated into a prestack-migrated CO panel. To account for an irregular acquisition geometry, the traces are weighted again by the midpoint increment of their neighboring traces. But now, only traces inside the current offset bin are considered for the calculation of $\Delta\xi$ as is depicted in Figure 2.

The determination of the local trace weighting factor becomes more tedious in 3D. For the estimation of $\Delta\xi_1\Delta\xi_2$ we have to find an area that describes the distribution of neighboring traces. Canning and Gardner (1998) have shown that a very suitable measure for this local trace weighting factor is the the Voronoi cell (Voronoj, 1908). Voronoi cells can be constructed making use of a Delaunay triangulation (Delaunay, 1934) for the considered point set. In the poststack case, this point set consists of all shot/receiver locations
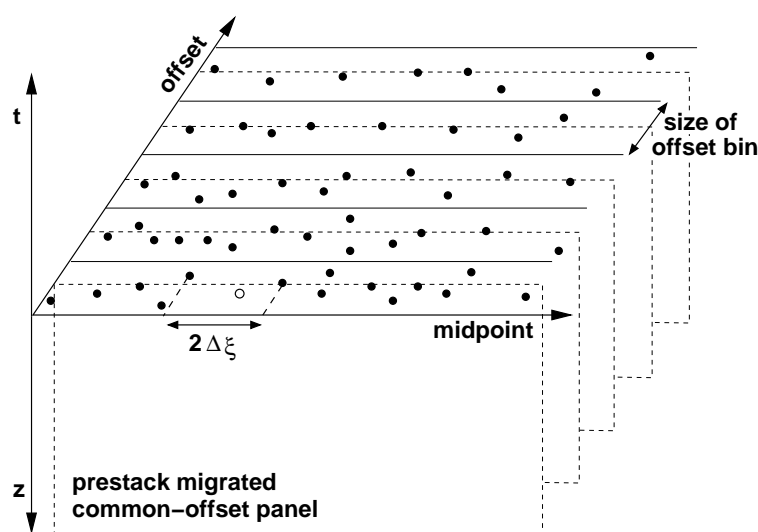
Figure 2: Determination of the local trace weighting factor $\Delta\xi$ for 2.5D prestack (common-offset) migration. For the trace denoted by the circle, $\Delta\xi$ is set to half the midpoint distance between its neighboring traces in the corresponding offset bin. Points denote trace positions.
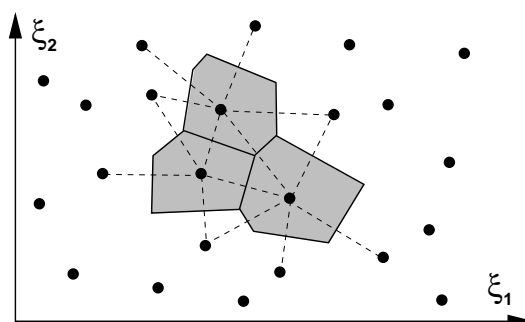

Figure 3: Voronoi cells. The points denote trace positions while the dashed lines denote some edges resulting from a Delaunay triangulation. The shaded areas are the Voronoi cells. The boundaries of a Voronoi cell are formed by the perpendicular bisectors to the edges containing the considered point.

of the 3D zero-offset (ZO) section to be migrated. The resulting triangles have the property that no points are located inside the circle through the three vertices of any such triangle. To obtain the Voronoi cell for a selected trace position, we construct the perpendicular bisectors to the edges containing the considered point. The intersection points of these bisectors are the vertices of the searched for Voronoi cell (Figure 3). In a descriptive way, the Voronoi cell for some input trace position consists of all points in the ξ_1-ξ_2-plane that are closer to the current trace location than to any other. For 3D prestack migration, the above considerations for the poststack case have to be extended similarly as for the previously discussed 2.5D situation (Jousset et al., 1999). Compared to the overall computational costs of migration the estimation of Voronoi cells is cheap and many sophisticated algorithms exist for this purpose. Therefore, they are a suitable tool to minimize the effects of an irregular acquisition geometry on the migration output.

Handling of topography

The true-amplitude weight functions in equations (1) and (2) depend, among other quantities, on the ray take-off and ray emergence angle, measured versus the normal vector to the measurement surface. For a 2.5D migration, the topographic variations along the acquisition line can be efficiently described by means of a spline interpolation which provides the necessary dip of the surface topography at every shot/receiver
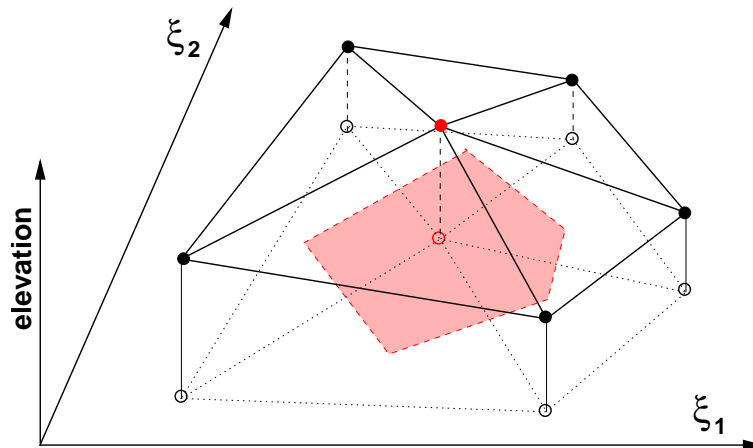
Figure 4: Sketch of a subset of a Delaunay triangulation result.

location. Unfortunately, a spline interpolation is very costly in case of 3D processing. Moreover, most spline interpolation implementations require lattice points distributed regularly in the ξ_1-ξ_2-plane which would require a regularization prior to migration for the considered irregular geometries. Therefore, we describe the measurement surface in a different way in the 3D case, making use of the Delaunay triangulation that we perform anyway in order to calculate the weighting factor $\Delta\xi_1\Delta\xi_2$. The result of this triangulation process, a selected midpoint together with its nearest neighbors, is depicted in Figure 4. For the calculation of the Voronoi cells (the shaded area in the ξ_1-ξ_2-plane) the elevation of the input points was ignored. In the poststack case these points correspond to physical shot/receiver positions. If we take their elevation into account, the resulting triangles (solid lines in Figure 4) approximate the actual measurement surface. The normal vector $\vec{n}$ at a selected vertex can then be estimated from the normal vectors of the adjacent triangles by means of weighted interpolation:

$$\vec{n} = \sum_i w_i \, \vec{n}_i \, , \quad i = 1 \ldots n \, . \tag{6}$$

The normal vectors $\vec{n}_i$ of the n adjacent triangles can easily be determined from two edges of the respective triangle. In order to take into account the irregular distribution of input points, the weight w_i can be chosen inversely proportional to the area of the ith triangle.

DATA EXAMPLE

To test 2.5D true-amplitude migration applied directly to data recorded with an irregular acquisition geometry on a non-flat topography, we made use of the simple synthetical model that is shown in Figure 5. This model consists of two homogeneous layers separated by a horizontal interface at a depth of $z = 1$ km. The p-wave velocities of these layers are $v_{p_1} = 2$ km/s and $v_{p_2} = 3$ km/s, respectively. The density is constant in the overall model.

2.5D poststack migration

As input for a poststack migration, the ZO section shown in Figure 6 was calculated by means of dynamic ray tracing. For this purpose, shots were randomly placed on the curved measurement surface in such a way that the resulting average trace spacing is 10 m. This seismogram was then migrated directly from topography. The local dip of the topography that enters into the true-amplitude weight function is calculated on the fly during migration, making use of a spline interpolation. To obtain the migrated image depicted in Figure 7a), the input traces where additionally weighted by the local trace increment determined by means of equation (5). Approximating $\Delta\xi$ in equation (4) by the constant average trace increment is not sufficient as can be seen from Figure 7b) where the resulting acquisition footprint distorts the reflector image. If we
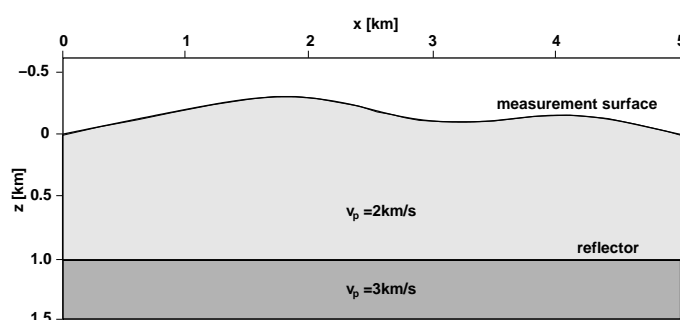
Figure 5: Synthetic 2.5D model. Shots and receivers are randomly placed along the indicated measurement surface with an elevation that varies between 0 m and 310 m.
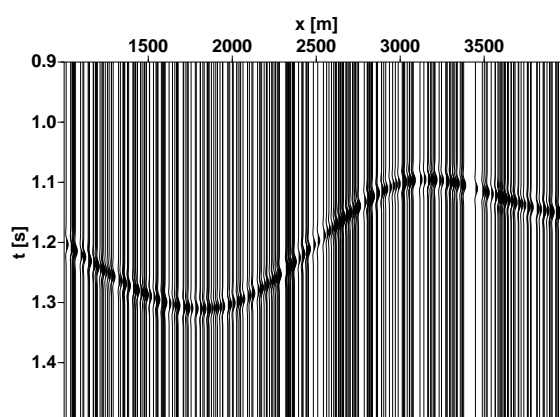

Figure 6: ZO section obtained by dynamic ray tracing in the model depicted in Figure 5. Shots/receivers were distributed randomly along the non-horizontal measurement surface. The effects of the irregular acquisition geometry and the topography are clearly visible.

look at the maximum amplitudes picked along the reflector in these two migrated images, the effects of the irregular acquisition geometry are even stronger (Figure 8). While the maximum amplitudes picked along the reflector image in Figure 7a) (dashed curve) are a very good measure of the actual normal-incidence reflection coefficient, the amplitudes in Figure 7b) (dotted curve) are strongly affected by the artifacts arising from the irregular distribution of traces in the input seismogram (Figure 6). Since the maximum amplitude is constant along the reflector image in Figure 7a) we can also conclude that the applied true-amplitude weight function has correctly removed the effects of the non-horizontal measurement surface.

2.5D prestack migration

To test 2.5D true-amplitude prestack migration from topography for an irregular measurement geometry, we calculated a multicoverage dataset for the same synthetic depth model described above. Source/receiver pairs were randomly distributed along the topography in such a way that each offset bin (10 m) contains 300 traces. The resulting average midpoint increment in each bin is 10 m and the offsets range from 0 m to 1800 m. The acquisition geometry is depicted in Figure 9 were the trace locations are plotted as points in the midpoint-offset plane.

For the prestack depth migration, the input seismogram was divided into offset bins. As we have proposed, the input traces were weighted, in addition to the true-amplitude weight, by the local midpoint increment in the respective offset bin (see Figure 2). The final prestack migration result that is already stacked in the offset direction is displayed in Figure 10a), no acquisition footprint is visible. If the irregular acquisition geometry is ignored and the input traces are only weighted by the constant average midpoint
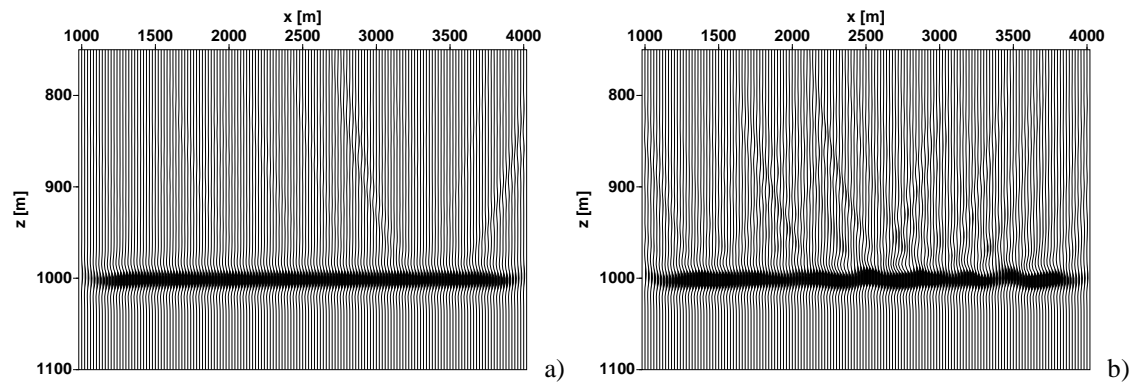
Figure 7: Migration of the ZO section displayed in Figure 6. The input traces where weighted by a) the local trace increment and b) the constant average trace increment of 10 m, respectively.
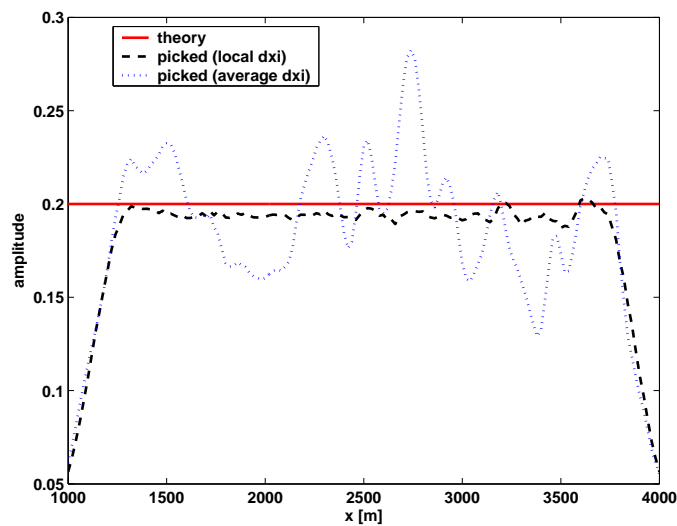

Figure 8: Comparison of amplitudes after true-amplitude migration. The dashed curve corresponds to the amplitudes picked in Figure 7a) while the dotted curve is obtained by picking the maximum amplitude along the reflector in Figure 7b). The analytically computed plane-wave normal-incidence reflection coefficient is 0.2 (solid line).
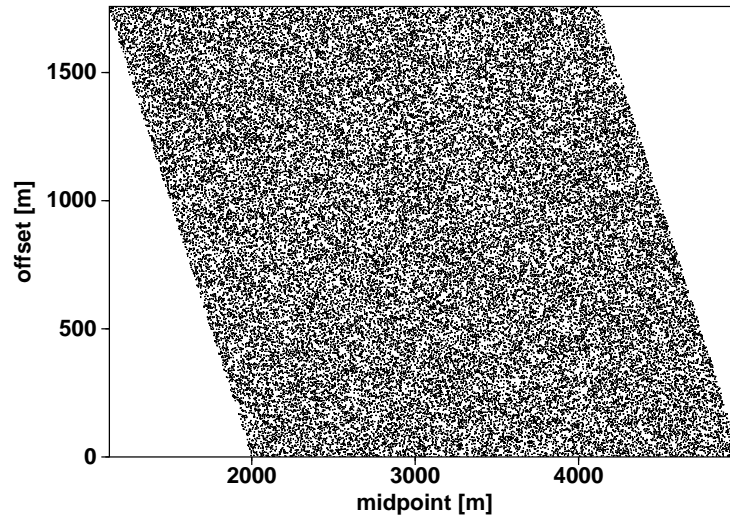
Figure 9: Irregular 2.5D multicoverage dataset: traces denoted by dots are randomly distributed in the midpoint-offset plane in such a way that each offset bin (10 m) contains 300 traces.
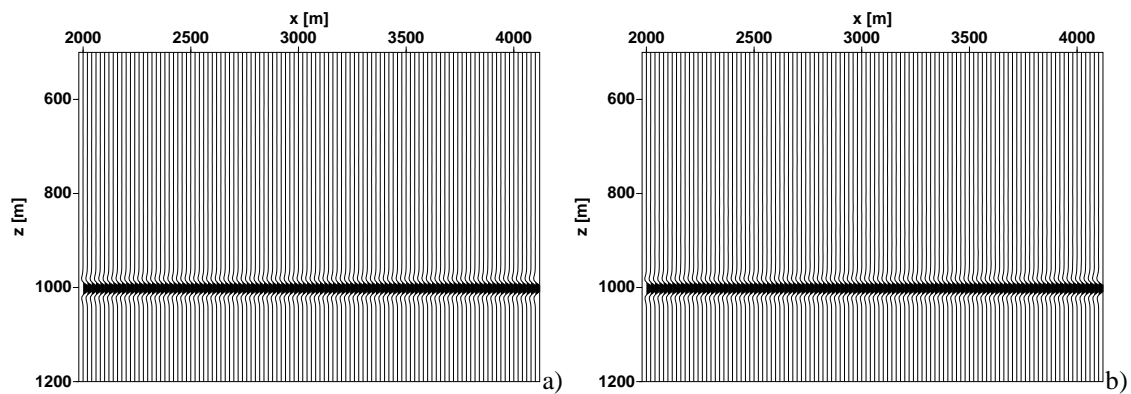

Figure 10: Prestack migration result of the irregular multicoverage dataset; all common-offset migrated panels were stacked along the offset axis. The input traces where weighted by a) the local trace increment and b) the constant average trace increment of 10 m, respectively.

increment in the offset bins, the resulting, stacked, migration output is Figure 10b). As there is no visible difference between these two images the determination of the local midpoint increment may seem to be unnecessary. The situation is, however, different when looking at individual CO-migrated panels (Figure 11) or common-image gathers (CIGs) (Figure 12) before stacking the CO-migrated panels. These images are strongly affected by artifacts if the irregular geometry is not accounted for. AVA/AVO curves are obtained by picking the amplitudes along events in CIGs. Doing this for the CIGs in Figure 12a) and b) yields the values depicted in Figure 13 by circles and crosses, respectively. We can clearly observe the effects of the acquisition footprint in Figure 12b) while the amplitudes picked in Figure 12a) are very close to the AVA curve computed analytically by means of the Zoeppritz equation (Zoeppritz, 1919).

3D poststack migration

To test 3D poststack migration of data recorded with irregular acquisition geometry on topography, we extended the model shown in Figure 5 identically in the y-direction perpendicular to the seismic line. The 3D ZO seismogram consists of 45,030 traces that are randomly distributed on the curved measurement surface. The shot coordinates are shown in Figure 14. One x-panel of the poststack migration result is
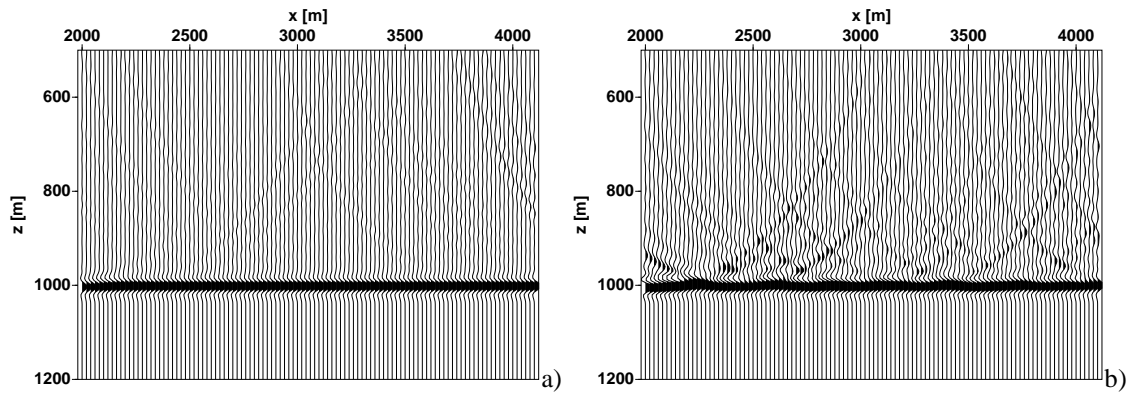
Figure 11: One CO-migrated panel (offsets between 200 m and 210 m) of the irregular multicoverage seismogram. The input traces where weighted by a) the local midpoint increment and b) the constant average midpoint increment of 10 m, respectively.
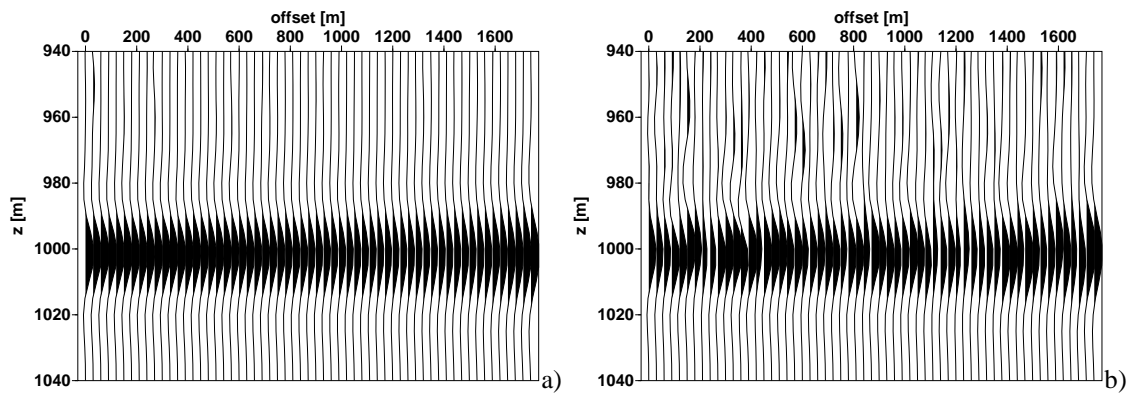

Figure 12: CIGs at x=2500 m after prestack migration of the irregular multicoverage seismogram. The input traces where weighted by a) the local trace increment and b) the constant average trace increment of 10 m, respectively.
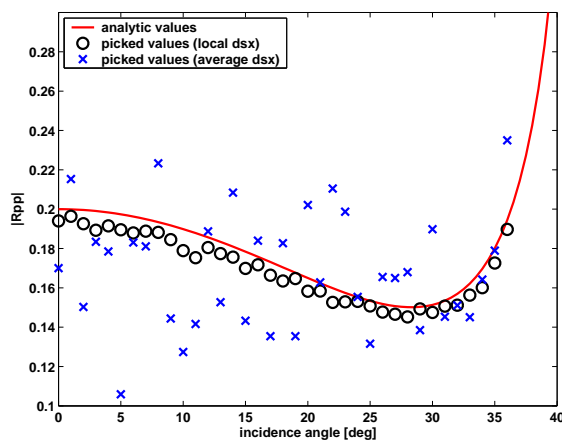

Figure 13: Comparison of analytically computed AVA curve (solid line) with amplitudes picked in the CIGs displayed in Figure 12a) (circles) and 12b) (crosses). For displaying purpose, the offset was transformed to incidence angle.
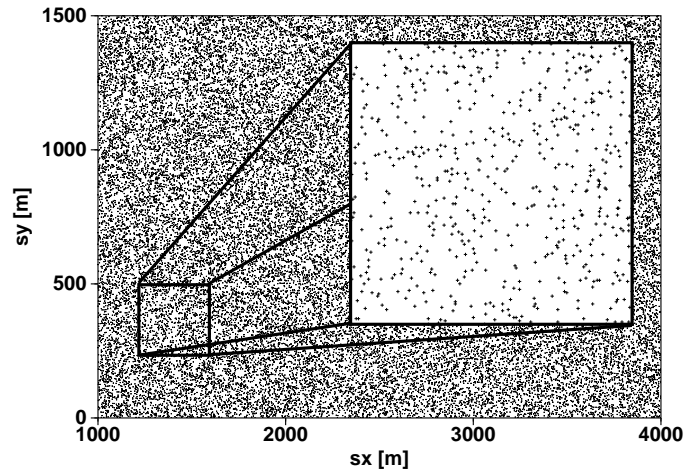
Figure 14: Location of shots in the irregular 3D ZO seismogram. The box on the upper righthand side is a zoom of the region $1250\,\text{m} < \text{sx} < 1500\,\text{m}$, $250\,\text{m} < \text{sy} < 500\,\text{m}$. 45,030 traces are randomly distributed over an area of $4.5\,\text{km}^2$, resulting in an average $\Delta\xi_1\Delta\xi_2$ of $100\,\text{m}^2$.
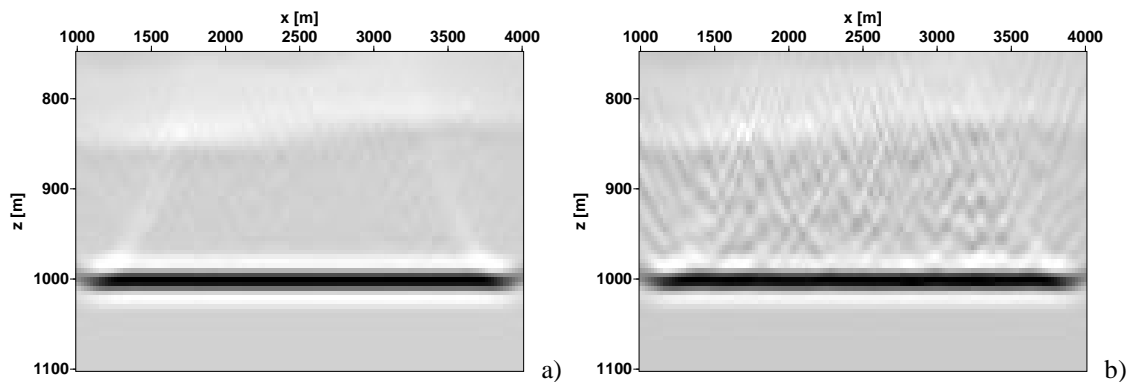

Figure 15: One x-panel of the 3D poststack migration result. Input traces were weighted by a) the area of their Voronoi cell and b) the constant average value $100\,\text{m}^2$.

shown in Figure 15a). To obtain this image, the input traces were weighted, apart from the true-amplitude weight function, by the area of their Voronoi cell. In addition, the result of the intermediate Delaunay triangulation was utilized to compute the normal vector to the measurement surface which enters into the true-amplitude weight. As in the 2.5D case, ignoring the irregular distribution of input traces leads to artifacts which severely degrade the migrated image, see Figure 15b). These artifacts also affect the amplitudes in the migration result (see Figure 16) and may lead to a misinterpretation of the visible amplitude anomalies. The maximum amplitude picked along the reflector in Figure 15a) is constant and close to the normal-incidence plane-wave reflection coefficient of 0.2, no distortion due to the non-flat topography or the irregular acquisition geometry is visible. The relative amplitude error, however, is larger than in case of the 2.5D migration (Figure 8). The reason for this difference is that in this case the analytical approximation of the integral in the out-of-plane direction in equation (1) by means of the stationary phase method (yielding equation (2)) is more accurate than its numerical approximation.

CONCLUSIONS

Kirchhoff migration is a very flexible migration method that can directly handle irregular measurement geometries and non-flat measurement surfaces. Using a simple synthetic data example, we have shown that migration applied directly from topography to data recorded with irregular acquisition geometries does not
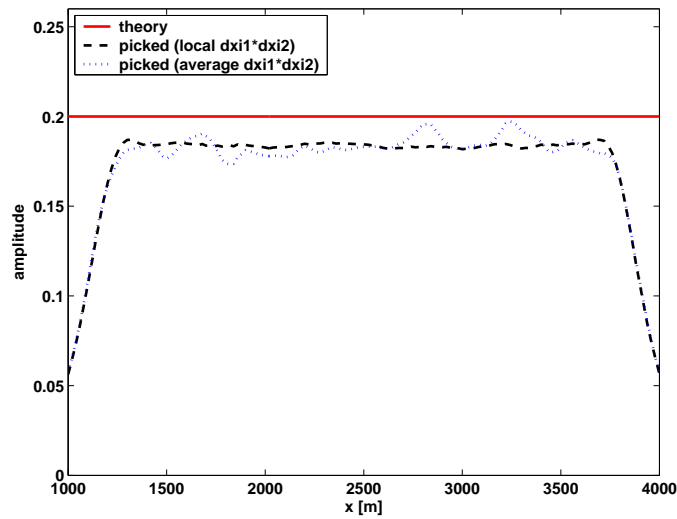
Figure 16: Comparison of amplitudes after 3D poststack true-amplitude migration. The dashed curve corresponds to the amplitudes picked in Figure 15a) while the dotted curve is obtained by picking the maximum amplitude along the reflector in Figure 15b). The analytically calculated plane-wave normal-incidence reflection coefficient is 0.2 (solid line).

only yield a kinematically correct image of the subsurface but is also able to relate the output amplitudes to the angle-dependent reflection coefficient. Prerequisite for accurate and clear migration results is that the applied true-amplitude weight function honors the elevation and local dip of the topography. Acquisition footprints affecting the image quality and the amplitudes along reflectors in the migration result can be minimized by weighting the input traces with an additional quantity describing the local acquisition geometry. In the 2.5D case, a suitable quantity for this is the midpoint increment of neighboring traces. For 3D migration, input traces should be weighted by the area of their Voronoi cell. In this way, amplitude analyses after migration are improved, yielding more reliable information to estimate physical properties of the subsurface.

REFERENCES

Bleistein, N. (1999). Hagedoorn told us how to do Kirchhoff migration and inversion. *The Leading Edge*, 18:918–927.

Canning, A. and Gardner, G. (1998). Reducing 3-D acquisition footprint for 3-D DMO and 3-D prestack migration. *Geophysics*, 63:1177–1183.

Delaunay, B. (1934). Sur la sphère vide. *Otdelenie Matematicheskii i Estestvennyka Nauk*, 7:793–800.

Gray, S., Etgen, J., Dellinger, J., and Whitmore, D. (2001). Seismic migration problems and solutions. *Geophysics*, 66:1622–1640.

Gray, S. and Marfurt, K. (1995). Migration from Topography: Improving the Near-Surface Image. *Can. J. Expl. Geophys.*, 31:18–24.

Hagedoorn, J. (1954). A process of seismic reflection interpretation. *Geophys. Prosp.*, 2:85–127.

Hertweck, T., Jäger, C., Goertz, A., and Schleicher, S. (2003). Aperture effects in 2.5D Kirchhoff migration: A geometrical explanation. *Geophysics*, 68(5):1673–1684.

Jäger, C., Hertweck, T., and Spinner, M. (2003). True-amplitude Kirchhoff migration from topography. In *Expanded Abstracts*. 73rd Ann. Internat. Mtg., Soc. Expl. Geophys. Session MIG 2.1.

Jousset, P., Thierry, P., and Lambaré, G. (1999). Reduction of 3-D acquisition footprints in 3-D migration/inversion. In *Expanded Abstracts*. 70th Ann. Internat. Mtg., Soc. Expl. Geophys. Session SPRO 11.1.

Jousset, P., Thierry, P., and Lambaré, G. (2000). Improvement of 3D Migration/inversion by reducing acquisition footprints: application to real data. In *Expanded Abstracts*. 70th Ann. Internat. Mtg., Soc. Expl. Geophys. Session MIG 5.5.

Martins, J., Schleicher, J., Tygel, M., and Santos, L. (1997). 2.5-D True-amplitude Migration and Demigration. *J. Seis. Expl.*, 6:159–180.

Newman, P. (1975). Amplitude and Phase Properties of a Digital Migration Process. In *Extended Abstracts*. Europ. Assoc. Expl. Geoph. (Republished in: First Break, 8:397-403, 1990).

Schleicher, J., Tygel, M., and Hubral, P. (1993). 3-D true-amplitude finite-offset migration. *Geophysics*, 58:1112–1126.

Schneider, W. (1978). Integral Formulation for Migration in Two and Three Dimensions. *Geophysics*, 43:49–76.

Spinner, M. (2003). True-amplitude Kirchhoff migration from topography – theory and application. Master's thesis, Karlsruhe University.

Voronoj, G. (1908). Nouvelles Applications des Paramètres Continus à la Théorie des Fores. Deuxième Mémoire. Recherches sur les Parallélloèdres Primitifs. *J. Pure Appl. Math.*, 134:198–287.

Zoeppritz, K. (1919). Erdbebenwellen VII: Über Reflexion und Durchgang seismischer Wellen durch Unstetigkeitsflächen. *Nachrichten der Königlichen Gesellschaft der Wissenschaften zu Göttingen*, pages 66–84.